Liquid-vapor phase transition and droplet formation by subpicosecond laser heating

B. Chimier[1,2,*] and V. T. Tikhonchuk[2]
[1]*Laboratoire Lasers, Plasmas et Procédés Photoniques, Faculté des Sciences de Luminy, 13288 Marseille, France*
[2]*Centre Lasers Intenses et Applications, Université Bordeaux 1-CEA-CNRS, 33405 Talence Cedex, France*
(Received 30 December 2008; revised manuscript received 8 April 2009; published 11 May 2009)

The expansion of a thin metallic layer isochorically heated by a subpicosecond laser pulse is studied theoretically and numerically. An analytical model that accounts for the liquid-vapor phase transition in expanding flow is developed. Numerical simulations performed for an aluminum target that is described by a multiphase equation of state confirm the analytical model. A repartition of the liquid and vapor phases in the expanding cloud is studied and the expressions for sizes of liquid droplets formed in the relaxation process are obtained. These estimates are in agreement with recent experimental and numerical results.

DOI: 10.1103/PhysRevB.79.184107 PACS number(s): 47.35.−i, 64.70.fm, 64.30.Ef, 79.20.Ds

I. INTRODUCTION

Subpicosecond laser pulses offer numerous advantages for material processing. Having pulse duration shorter than the electron-ion temperature relaxation time, such pulses can heat a thin layer at the target surface to high temperatures, while keeping its density unchanged. Properties of such states of a warm dense matter are not known and are a subject of intense studies.[1–10] Moreover, the ejected matter does not interact with the laser pulse. Expansion and decomposition of the heated matter occur later in time and present an interest for nanoparticle synthesis and production of thin films.[11–13] However, the process of expansion of heated material proceeds in the time scale shorter than a few ns. The phase transitions in fast evolving matter are poorly understood. Recent studies[5,7] have shown that there are two qualitatively different ablation processes. For laser fluences close to the ablation threshold and very short laser pulses, the ions in the surface layer remain cold and they are removed by the electron-driven process. As soon as the average electron energy gained from the laser pulse becomes higher than the ion binding energy, the electrons pull out cold ions from the surface. For higher laser fluences and longer pulses, the ion heating time becomes shorter than the ablation time. Then the hydrodynamic ablation process becomes more important. The matter in the laser heated layer is transformed in the vapor phase and then expands under its own the thermal pressure.

The objective of this paper is to consider the hydrodynamic expansion of a thin hot surface layer under the conditions where the phase transitions take place during the expansion and some of material finds itself in a liquid phase surrounded by vapors. We evaluate the relative mass of the liquid and vapor phases as a function of initial heating conditions and estimate the characteristic size of liquid droplets and their velocity.

Let us consider a homogeneous and isochoric heating of a thin layer at the surface of a metal sample. The temperature and the pressure in this layer increase sharply during the heating process, while the density remains approximately constant, equal to the initial density. We assume that at the end of the laser pulse, the matter in this heated layer is in a liquid state. The pressure relaxation induces an expansion of this surface layer into vacuum, and creation of a shock wave, which propagates into the target. During the relaxation process, the density drops down and a part of liquid matter can be converted into vapor. In first approximation, one can neglect the heat transport processes and consider an isentropic expansion process. The phase transition can be considered as a fast process, which takes place locally during the two-phase system expansion. That means we suppose that the system is all time and everywhere in the local thermodynamic equilibrium. In particular, during the expansion in the two-phase domain, the pressures of the liquid and vapor phases are equal to the saturated pressure on the binodal for a given temperature, $P_l(T)=P_v(T)=P_{\mathrm{sat}}(T)$.

In the case of a relatively mild heating, where the expansion drives the heated matter to the binodal at a density larger than the critical density, the matter is in a liquid phase when it enters in the two-phase region. The slope of the adiabat at the binodal changes abruptly and the sound velocity, $c_s=(\partial P/\partial\rho)_S^{1/2}$, exhibits a dramatic fall. The isentropic expansion is then split into two rarefaction waves: first, which evolves in the liquid phase, and second, which evolves in the two-phase state, where the sound velocity is much lower. These two rarefaction waves are separated by a liquid layer of a constant density.[1–3] As a result of expansion of the heated layer into vacuum, a shock wave is launched into the cold matter.[14,15] The relaxation in the cold matter behind the shock forms a second liquid layer of a constant density along with two other layers where the matter is in a mixed liquid-vapor state. During the expansion phase, these liquid layers are partially vaporized and partially transformed into liquid droplets.

Such a complex structure of expansion flow with the liquid-vapor phase transition was studied in Refs. 1–3 in the case of a homogeneous and isochoric heating. The main results of these studies are recalled in Sec. II A. The results concerning propagation of the shock wave into the target, which is a classical hydrodynamic problem,[14,15] are presented in Sec. II B. These two models are coupled in Sec. II C to explain the isentropic relaxation of a high-pressure layer in a cold matter and in vacuum. We show that two homogeneous layers of liquid matter appear in the expanding cloud, while a part of matter evolves into a liquid-vapor mixture. These results are confirmed by numerical simulations

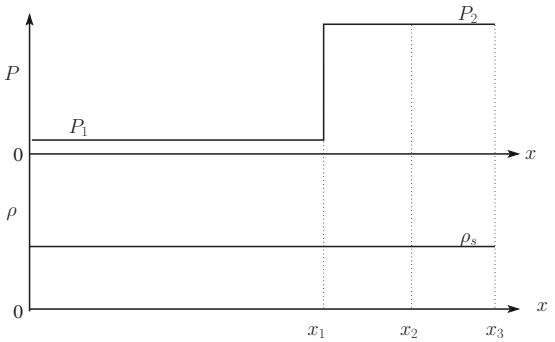

FIG. 1. Density and pressure profiles in the target after the heating.

performed with a thick aluminum target and a thin high-pressure layer on its surface (Sec. III). Estimates of the liquid layer lifetimes are performed in Sec. IV A. The sizes of ejected droplets are estimated from the point of view of stability of expanding layer and the energy balance acting on each droplet in Sec. IV B. The average droplet size decreases as the initial pressure in the heated layer increases and our results show that the biggest droplets are formed near the target surface. These conclusions are compared with the recent experimental and numerical studies.[12,13,16–18]

II. EXPANSION OF A HIGH-PRESSURE LAYER

The problem of expansion of a high-pressure layer on a free surface consists of two phenomena: the rarefaction wave emerging from the surface in vacuum and the shock wave propagating into the target. To simplify the problem, we assume that the thermal conduction can be neglected during the expansion process, $c_s t > \sqrt{\chi t}$ (where χ is the thermal conductivity), and that initially the pressure is homogeneous in the heated layer. Figure 1 presents the density and pressure profiles when the heating is terminated but the expansion is not started yet. The heated layer of size $2h$ is between points x_1 and x_3, where the pressure is P_2. Point x_2 is in the middle of this layer. The cold matter is in the interval between 0 and x_1, where the pressure is $P_1 \ll P_2$. The vacuum is on the right side of x_3. The density is homogeneous, $\rho=\rho_s$.

We assume that the high-pressure layer is in a liquid state and at $t=0$ two rarefaction waves are launched from edges x_1 and x_3 toward center x_2. Because of the symmetry of the problem, in the beginning we can divide the layer (x_1,x_3) into two equal parts of thickness h, assuming a rigid boundary at x_2. The first half-layer (x_2,x_3) expands in vacuum, while the second half-layer (x_1,x_2) expands into the cold matter.

A. Expansion of a finite-thickness layer in vacuum

First, let us consider the layer of thickness h between x_2 and x_3 that expands in vacuum. As the heat conductivity is neglected, the expansion of this layer is treated as an isentropic process and it is described by a centered rarefaction wave.[14,15] The equations of gas dynamics in one dimension read

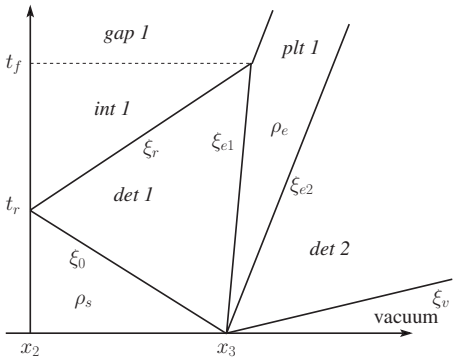

FIG. 2. Characteristics of the expanding matter, which was initially between x_2 and x_3.

$$\frac{\partial \rho}{\partial t} + u\frac{\partial \rho}{\partial x} + \rho\frac{\partial u}{\partial x} = 0, \tag{1}$$

$$\frac{\partial u}{\partial t} + \frac{c_s^2}{\rho}\frac{\partial \rho}{\partial x} + u\frac{\partial u}{\partial x} = 0, \tag{2}$$

where ρ and u are, respectively, the density and the velocity; $c_s=(\partial P/\partial\rho)_S^{1/2}$ is the sound velocity; and P is the pressure. These equations should be complemented by the equation of the adiabat $S(P,\rho)=S_0$ (where S_0 is entropy at the beginning of expansion), which can be written in the form $P=P(\rho)$.

Figure 2 shows the characteristics of the expanding layer. The rarefaction process consists of two stages: (1) propagation of the rarefaction wave *det 1* across the target and formation of a plateau *plt 1* of a density ρ_e due to the phase transition and (2) interaction of the forward and reflected waves in *int 1* and formation of a density gap *gap 1*.

The rarefaction wave propagates into the target with the sound velocity $c_0=c_s(\rho_s)$ in the unperturbed material. This wave is reflected at point x_2 at the time $t_r=h/c_0$ due to the collision with the opposite traveling rarefaction wave originated from x_1. Before t_r, the flow is described by a centered rarefaction wave in a semi-infinite layer and it is self-similar. The self-similar variable is $\xi=x/t$, and the solutions to Eqs. (1) and (2) for isentropic expansion are

$$\xi = u - c_s, \quad u = \int_{\rho}^{\rho_s} \frac{c_s}{\rho} d\rho. \tag{3}$$

The structure of rarefaction flow is more complicated if the expansion adiabats cross over the binodal at a temperature T_e smaller than the critical temperature and enter the two-phase region. There, the matter is in a heterogeneous phase of liquid and gas, and the sound velocity is lower. This splits the rarefaction wave into two parts: first part, which evolves in the liquid state (*det 1* in Fig. 2), and a second part (*det 2*), which evolves in the two-phase state.

At the crossing point e of the adiabat and the binodal, the fluid velocity must be continuous and $u_{e1}=u_{e2}=u_e$ (u_{e1} is the velocity at point e on the liquid state and u_{e2} is velocity at e on the two-phase region). According to Eq. (3), this implies a discontinuity in the self-similar variable ξ. As c_{e1} is greater

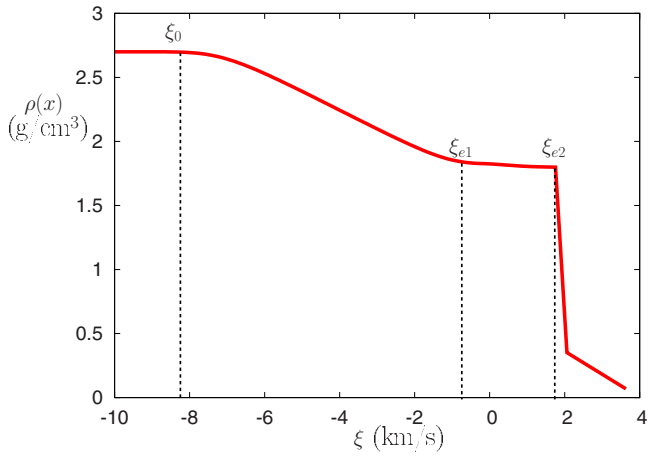

FIG. 3. (Color online) Density profile in the self-similar rarefaction wave of an aluminum target. The initial conditions are $T_s=0.52$ eV and $\rho_s=2.7$ g/cm^3.

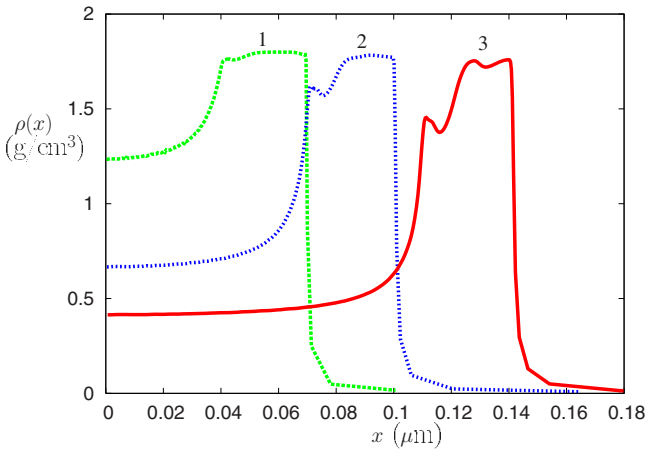

FIG. 4. (Color online) Density profiles in isentropic expansion of an aluminum target with a phase transition for times $t=15$ ps (1), 30 ps (2), and 50 ps (3).

than c_{e2}, from Eq. (3) $\xi_{e1}<\xi_{e2}$ and the first and second parts of the rarefaction wave are not immediately adjacent one to another. They are separated by a plateau[1–3] (*plt 1* in Fig. 2) of a uniform density ρ_e, which moves with the velocity u_e. The width of the plateau is $h_{p1}=(\xi_{e2}-\xi_{e1})t=(c_{e1}-c_{e2})t$, and it increases with time.

Figure 3 represents the density profile as a function of the self-similar variable ξ. The calculations were performed with an aluminum target at the initial density $\rho_s=2.7$ g/cm^3 and the initial pressure $P_s=26$ GPa. Here, ξ_0 is the value of ξ at the front of the rarefaction wave in the unperturbed material and ξ_{e1} and ξ_{e2} are, respectively, the values of ξ on the liquid state and in the two-phase region at point e.

According to Fig. 3, the expansion flow is divided into four parts. For $\xi<\xi_0$, the density is constant and equal to ρ_s. This part corresponds to the unperturbed material. For $\xi_0<\xi<\xi_{e1}$, the density decreases from ρ_s to $\rho_e=1.8$ g/cm^3. In this part, the matter is in the liquid state and the expansion corresponds to the first portion of the rarefaction wave *det 1*. For $\xi_{e1}<\xi<\xi_{e2}$, the density is constant and is equal to ρ_e. This part corresponds to the plateau *plt 1* of a constant density. For $\xi_{e2}<\xi$, the density decreases sharply. It is smaller than ρ_e and the matter is in the two-phase state. In this part, the expansion corresponds to the second portion of rarefaction wave *det 2*.

At the time $t_r=h/c_0$, the rarefaction is reflected and it interacts with the incident wave. The flow is divided into two parts: in the interval $x_r(t)<x<x_{e1}(t)$ there is one simple wave (*det 1* in Fig. 2), while the incident and reflected waves interact in $0<x<x_r(t)$ (*int 1* in Fig. 2). To obtain a qualitative picture of the flow in the interaction zone, let us consider the material as an ideal gas with adiabatic index γ. The problem of the interaction of an incident and reflected waves was solved in Ref. 14 and the solution reads

$$c=\frac{h}{t}\left(\frac{t}{t_r}\right)^{(3-\gamma)/(\gamma+1)}, \quad \rho=\rho_s\left(\frac{t_r}{t}\right)^{4/(\gamma+1)}, \quad u=\frac{x}{t}+\frac{h}{t}\left(\frac{t}{t_r}\right)^{(3-\gamma)/(\gamma+1)}. \tag{4}$$

According to Eq. (4), the density in the interaction region does not depend on coordinate and it decreases with time.[1–3] The reflected wave reaches the plateau at the time $t_f=t_r(\rho_s/\rho_e)^{(\gamma+1)/4}$. At this time, the density is homogeneous and equal to ρ_e in the reflected wave and in the plateau.

The velocity, according to Eq. (4), is a linear function in the wave interaction region and it is constant in the plateau. Therefore, for $t>t_f$, the matter from the wave interaction region cannot enter in the plateau. The size of the plateau is maximum at t_f and it is $h_{p1}=(c_{e1}-c_{e2})t_f$. The density in the wave interaction region continues to decrease according to Eqs. (1) and (2) and it becomes smaller than ρ_e. A gap is formed between the target backside and the plateau (*gap 1* in Fig. 2).

The flow at $t>t_f$ corresponds to a liquid layer of a constant density ρ_e (plateau), separated from the rest of the target and flying with a constant velocity. In front of the plateau, there is a low-density tail. Behind it, there is a gap made of a mixture of liquid and vapor. The rarefaction front propagates into the plateau with the velocity c_{e2} and its thickness decreases with time. This is a slow process as the velocity c_{e2} is very small.

This general picture of a rarefaction wave in two-phase system can be better seen in numerical simulations. In the example shown in Fig. 4, the simulation was made with a thin aluminum target of thickness $h=40$ nm. The initial density and the initial temperature are, respectively, $\rho_s=2.7$ g/cm^3 and $P_s=26$ GPa. The sound velocity in the unperturbed material is $c_0=7.17$ km/s. The density profiles are shown for times greater than t_f. The density in the gap decreases from 1.3 g/cm^3 at 15 ps to 0.4 g/cm^3 at 50 ps. The density in the plateau is homogeneous and it is equal to $\rho_e=1.8$ g/cm^3. The outer region, where the density decreases sharply, is the external part of the rarefaction wave, which is also in the two-phase state.

B. Relaxation in the cold matter

Here, we consider the matter in the interval between 0 and x_2 in Fig. 1. The pressure jump at x_1 launches a shock wave

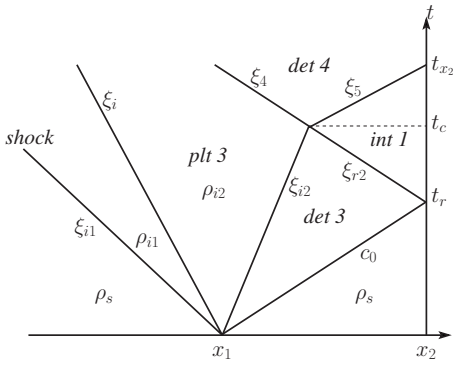

FIG. 5. Characteristics of the relaxation in the cold matter.

into the cold matter and a rarefaction wave into the hot layer.

Figure 5 presents the relaxation characteristics in the cold matter. In the rarefaction wave (*det 3*), the density decreases and becomes smaller than ρ_s. The matter in the low-pressure area is compressed to a density ρ_{i1} greater than ρ_s, and a shock wave is launched. As the pressure is constant behind the shock wave,[14,15] the expansion of the high-pressure layer is limited and a plateau *plt 3* of a density $\rho_{i2} < \rho_s$ appears behind the compressed matter. The line ξ_i shows the position of the contact point between hot and cold matters.

The rarefaction wave *det 3* reaches x_2 at time t_r where it collides with *det 1* (see Fig. 2) and the two waves interact one with other. As it was explained in the previous section, in the interaction zone *int 1* the density is homogeneous and decreases with time. The interaction zone collides with the plateau *plt 3* at the time t_c and a new rarefaction wave appears between the plateau *plt 3* and the interaction area *int 1* (*det 4* in Fig. 5). When the rarefaction foot reaches x_2 at the time t_{x_2}, our artificial separation of the layers (x_1, x_2) and (x_2, x_3) is no longer valid. The subsequent analysis of expansion process is presented in the next section.

An analytical description of the relaxation process can be done for an ideal gas with the adiabatic index γ. Assuming that the pressure P_i in the compressed matter is greater than the pressure in the cold matter, $P_i \gg P_1$, the density and pressure behind the shock wave[14,15] can be expressed as

$$\rho_{i1} = \frac{\gamma+1}{\gamma-1}\rho_s, \quad P_i = \frac{\gamma+1}{2}\rho_s u_i^2, \tag{5}$$

where u_i is the matter velocity behind the shock. Because of the continuity of the matter, it is the same as the velocity in the plateau *plt 3*, $u_i = u_{i2}$. This velocity u_{i2} can be found considering the rarefaction wave *det 3*. As the expansion is isentropic, the pressure in the rarefaction wave *det 3* writes $P_i = P_2(\rho_{i2}/\rho_s)^\gamma$ and the velocity is

$$u_{i2} = -Nc_0\left[1 - \left(\frac{\rho_{i2}}{\rho_s}\right)^{1/N}\right], \tag{6}$$

where $N = 2/(\gamma-1)$ and $c_0 = \sqrt{\gamma P_2/\rho_s}$. Then, the density ρ_{i2} in the plateau *plt 3* is given by the polynomial equation

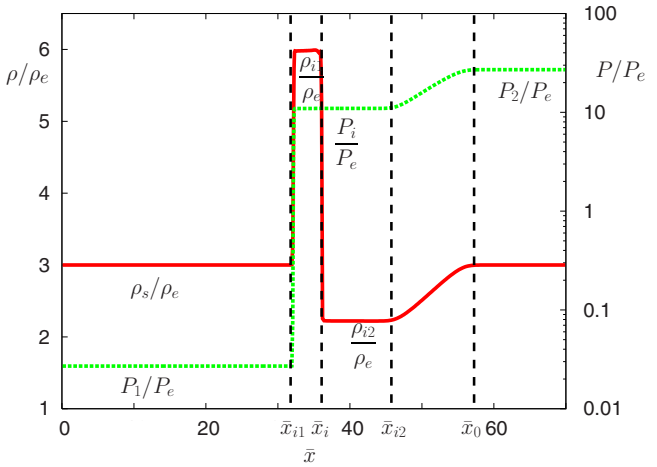

FIG. 6. (Color online) Density and pressure profiles at time $t = t_r/2$ during the relaxation in the cold matter considered as an ideal gas with $\gamma = 3$. The lengths are normalized by $\bar{c}t_r$, where $\bar{c} = \sqrt{P_e/\rho_e}$.

$$\left(\frac{\rho_{i2}}{\rho_s}\right)^\gamma - N\gamma\frac{\gamma+1}{\gamma-1}\left[1 + \left(\frac{\rho_{i2}}{\rho_s}\right)^{2/N} - 2\left(\frac{\rho_{i2}}{\rho_s}\right)^{1/N}\right] = 0. \tag{7}$$

Figure 6 presents the density and pressure profiles at the time $t = t_r/2$ during the relaxation of the heated layer in the cold matter for an adiabatic index $\gamma = 3$. Initially, the heated matter is localized between $\bar{x}_1 = 40$ and $\bar{x}_2 = 70$ where the pressure is $P_2 = 27P_e$, and the cold matter is between 0 and $\bar{x}_1$ where the pressure is $P_1 = 0.027P_e$. The density in the matter is $\rho_s = 3\rho_e$. Here, P_e is the pressure at the binodal crossing point.

At the time $t = t_r/2$, a part of matter, between $\bar{x}_{i1}$ and $\bar{x}_i$, is compressed to a density $\rho_{i1} = 6\rho_e$. Behind this region, between $\bar{x}_i$ and $\bar{x}_{i2}$, a plateau of a constant density $\rho_{i2} = 2.2\rho_e$ is appeared. In these two parts of the density profile, the pressure and velocity are constant and equal to $P_i = 11P_e$ and $u_{i2} = -0.26c_0$, respectively. The compressed matter corresponds to the cold matter, which was pushed by the relaxation of the heated layer, and the matter in the plateau corresponds to the heated matter, which was expanded to the pressure P_i.

Behind the plateau, between $\bar{x}_{i2}$ and $\bar{x}_0$, the density and the pressure decrease, respectively, from ρ_s to ρ_{i2} and from P_2 to P_i. This part corresponds to the heated matter, which expands into the cold matter (*det 3* in Fig. 5).

As in the previous section, the rarefaction wave front reaches x_2 at the time $t_r = h/c_0$. In the interaction zone (*int 1* in Fig. 5), the density is homogeneous and it decreases with time. At the time $t_c = t_r(\rho_s/\rho_{i2})^{(\gamma+1)/4}$, the density in *int 1* is equal to the density ρ_{i2} in the plateau *plt 3*.

For times $t > t_c$, the density in the wave interaction zone *int 1* continues to decrease and a rarefaction wave appears between the plateau *plt 3* and the wave interaction zone *int 1* (*det 4* in Fig. 5). The rarefaction front propagates into the plateau with the velocity $c_{i2} = c_0(\rho_{i2}/\rho_s)^\gamma$, and $\xi_4 = u_{i2} - c_{i2}$. The position of rarefaction wave foot is determined by using the Riemann invariants $J_\pm = u \pm Nc$ (Refs. 14 and 15), and the expressions of the velocity u and sound velocity c (4) in the wave interaction region (*int 1* in Fig. 5). It reaches point

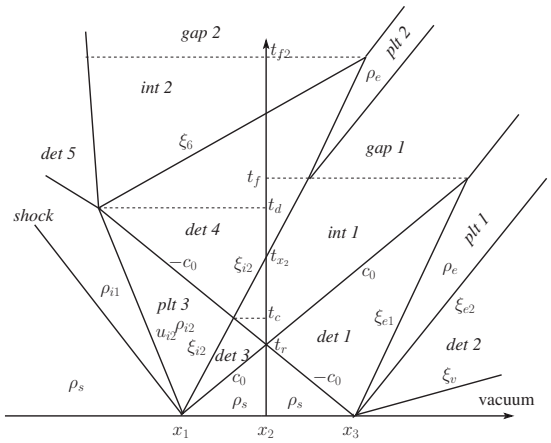

FIG. 7. Relaxation characteristics of a heated layer on a target surface.

x_2 at the time t_{x_2}. For $\gamma=3$, $\xi_5=\xi_{i2}=0.48c_0$ and $t_{x_2}=c_0t_r/\xi_{i2}$.

C. Relaxation of a high-pressure layer

We have seen that the relaxation of a hot layer induces a formation of a plateau of constant density from the vacuum side, while a shock wave is launched in the cold matter. Figure 7 presents the characteristics of the relaxation process within the heated layer.

The heated matter, initially in the interval x_1x_3, expands in vacuum and into the cold matter. Two rarefaction waves propagate into the heated matter (*det 1* and *det 3* in Fig. 7) with the velocity c_0. At time t_r, they reach the middle of the heated layer x_2.

The relaxation in the cold matter induces the formation of a shock wave, which compresses the cold matter to the density ρ_{i1}. Behind the compressed matter, a plateau (*plt 3* in Fig. 7) of the density $\rho_{i2}<\rho_s$ appears.

From the vacuum side, the phase transition induces a discontinuity of sound velocity, which splits the rarefaction wave into two waves: one evolves in the liquid matter (*det 1*) and another evolves in the two-phase state (*det 2*). They are separated by a plateau (*plt 1*) of a constant density ρ_e.

For times $t>t_r=h/c_0$, overlapping of two rarefaction waves *det 1* and *det 3* creates the interaction region *int 1* in Fig. 7, where the density is homogeneous and decreases with time. At the time t_c, the density in *int 1* is ρ_{i2}. As the time goes on, the interaction of *int 1* with the plateau *plt 3* creates the rarefaction wave *det 4* in Fig. 7. For $\gamma_1=3$, the front of *det 4* propagates into *plt 3* with the velocity $-c_0$, and the foot propagates with the velocity ξ_{i2}.

At the time t_d, the wave front of *det 4* reaches the compressed matter. A part of the rarefaction wave is transmitted into the compressed matter and a part is reflected. The reflected wave interacts with the incident wave in the interaction region *int 2* in Fig. 7.

At the time t_f, the density in the interaction region *int 1* is equal to the density ρ_e in the plateau *plt 1*. A first gap appears in the expanding cloud (*gap 1* in Fig. 7) as it was explained in Sec. II A.

As the matter is in the two-phase state in the *gap 1*, a discontinuity of sound velocity appears in the rarefaction wave *det 4*. The rarefaction is split into two waves, which are separated by a plateau of constant density ρ_e (*plt 2* in Fig. 7). The width of this plateau is $h_{p2}=(c_{e1}-c_{e2})(t-t_f)$ and it increases with time.

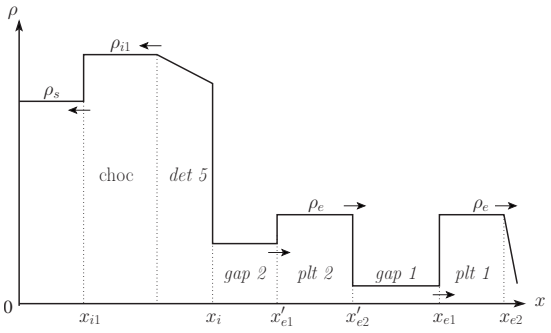

FIG. 8. Density profile at time $t>t_{f2}$. Arrows show the direction of motion of the corresponding fronts.

When the reflected wave in *int 2* reaches the plateau *plt 2* at time t_{f2}, the density is homogeneous and equal to ρ_e in the interaction region *int 2* and in the plateau *plt 2*. Similarly to what had happened in the interaction region *int 1*, the density in *int 2* continues to decrease and the matter enters in the two-phase state, where the matter is a heterogeneous mixture of liquid and vapor. A second gap appears in the expanding cloud between the compressed matter and the plateau *plt 2* (*gap 2* in Fig. 7). The plateau moves to the vacuum with the constant velocity $u_{e2}=2(c_{i2}-c_{e1})/(\gamma_1-1)$.

Figure 8 presents the density profile in the system at time $t>t_{f2}$. The expanding cloud includes four elements: two gaps, where the matter is a mixture of liquid and vapor, and two plateaus of liquid matter. As the time goes on, both plateaus move to the vacuum with constant velocities and density in both gaps continues to decrease.

The mass repartition in the different elements of the expanding cloud depends on the adiabatic index γ and the position of the intersection of the adiabat and the binodal. To obtain the mass repartition, one must use a more appropriate equation of state (EOS) than that of an ideal gas.

III. NUMERICAL SIMULATIONS OF THE RAREFACTION WAVE

As an example of two-phase rarefaction wave formation, we consider an aluminum target of 200 nm thickness. The initial pressure $P_1=10^{-4}$ GPa and the density $\rho_s=2.7$ g/cm^3. A thin layer of $h=40$ nm on its surface is heated to a pressure P_2. The simulations were performed for the three cases $P_2=20$, 26, and 43 GPa. The thermal conduction is neglected during the expansion process.

Figure 9 presents the phase diagram of aluminum calculated from the multiphase EOS by Bushman *et al.*[19] and three adiabats corresponding to given initial pressures. Each adiabat starts in the liquid state where the pressure is greater than the critical pressure (at point *C*) and its shape depends on P_2. The values of ρ_e, c_0, c_{e1}, and c_{e2} given by the EOS are presented in Table I.

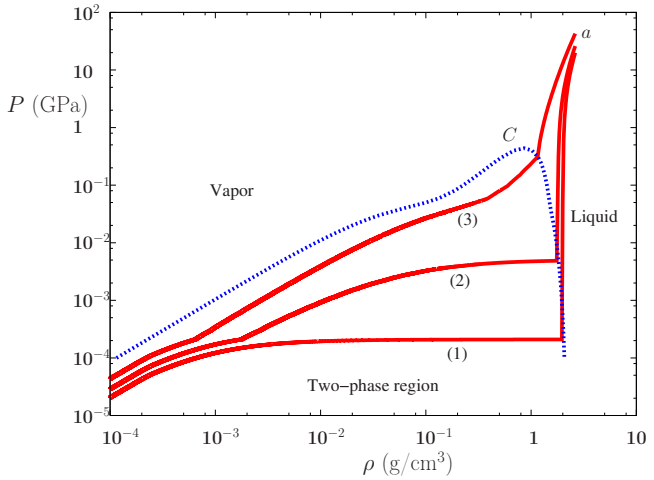

FIG. 9. (Color online) Adiabats of the aluminum in the (P,ρ) plane. The initial pressures at the starting point a are 20 GPa (1), 26 GPa (2), and 43 GPa (3). The dashed curve is the binodal and C indicates the critical point.

Each adiabat reaches the binodal where the pressure is smaller than the critical pressure. In the two-phase region, a part of the liquid is vaporized and vapor bubbles appear. Their growth during the expansion drives liquid to fragmentation and the two-phase system evolves to a heterogeneous mixture of liquid droplets surrounded by vapor.

The numerical results are in agreement with the general scenario described above. The heated matter expands into the vacuum and the cold matter. Two plateaus of constant density ρ_e and two gaps of density appear in the expanding cloud. The profiles of the density, pressure, and velocity for the case of the initial pressure of 26 GPa are presented in Fig. 10. The position of the high-pressure layer corresponds to the vertical dotted lines, between $x=160$ and 200 nm.

At the time of 3.1 ps [panel (a)], on the left side from the initial heated layer, the matter is compressed to the density $\rho=3.07$ g/cm^3 and a plateau of a density $\rho=2.4$ g/cm^3 is formed. In these two regions, the pressure is homogeneous and is equal to 13 GPa. The density plateau contains the heated matter, which was expanded to the pressure of 13 GPa. This region corresponds to the plateau *plt 3* in Fig. 7. Behind the plateau, the density decreases from 2.52 to 2.4 g/cm^3. This part corresponds to the rarefaction wave (*det 3* in Fig. 7).

To the right from the initial position of heated layer, a plateau of a constant density $\rho_e=1.8$ g/cm^3 and thickness $h_{p1}=9$ nm is formed. It splits the rarefaction wave into two

TABLE I. Values of the sound velocity and density on the binodal for the adiabats (1)–(3) in Fig. 9. The initial density is $\rho_s=2.7$ g/cm^3.

P_2 (GPa)	ρ_e (g/cm^3)	c_0 (km/s)	c_{e1} (km/s)	c_{e2} (km/s)
20	2	6.85	3.5	0.4×10^{-3}
26	1.8	7.17	3	4×10^{-3}
43	1.18	8	1.05	0.22

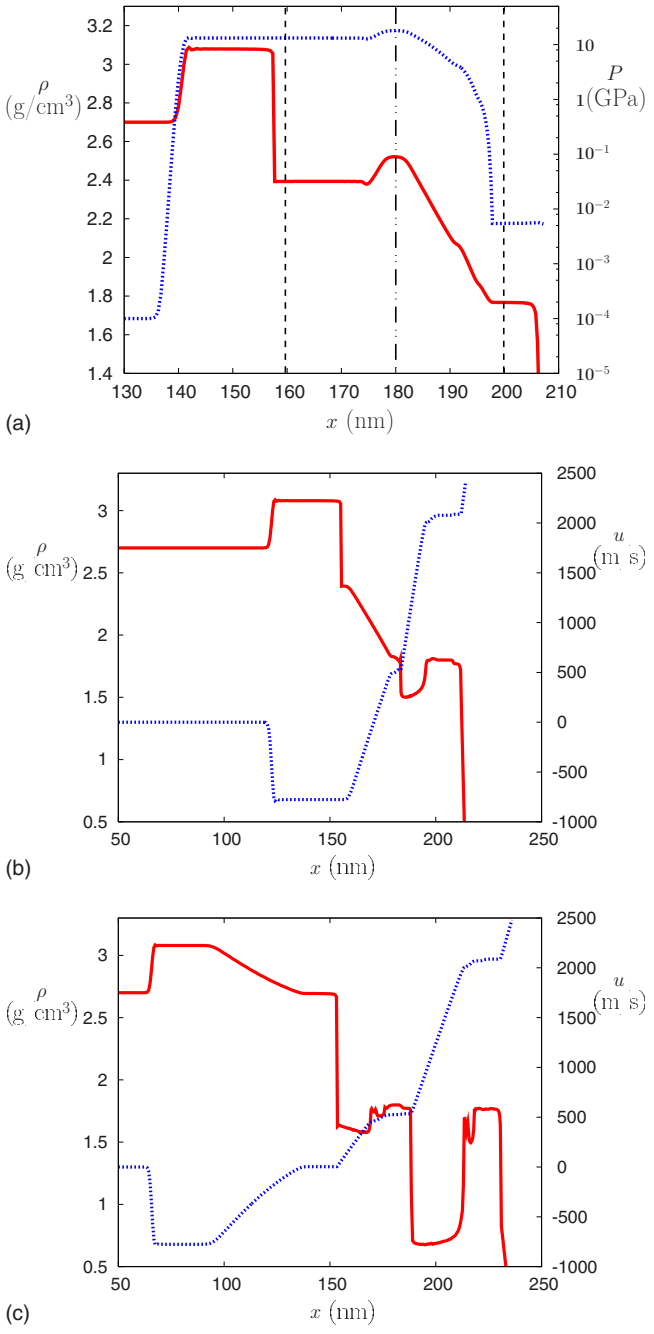

FIG. 10. (Color online) Profiles of the density (solid lines), pressure, and velocity (dotted lines) for the case of relaxation of a 40 nm high-pressure layer at the Al target surface. The initial pressure in the layer is 26 GPa. Panel (a) presents the density and pressure profiles at $t=3.1$ ps; panels (b) and (c) present the density and velocity profiles at $t=6$ and 15 ps, respectively.

parts: first, which evolves in the liquid matter, where $\rho>\rho_e$, and second, which evolves in the liquid-vapor mixture, where $\rho<\rho_e$. This plateau corresponds to *plt 1* in Fig. 7, and the two parts of the rarefaction wave correspond to *det 1* and *det 2*.

Between the rarefaction waves *det 1* and *det 3*, the density and the pressure are constant and smaller than the initial values ($\rho=2.52$ g/cm^3 and $P=18.8$ GPa). In this region, two rarefaction waves interact (for these initial conditions the

TABLE II. Simulation results for a 40 nm high-pressure layer relaxation for the adiabats (1)–(3) in Fig. 9. The initial density is $\rho_s = 2.7$ g/cm^3.

P_2 (GPa)	u_e (km/s)	t_f (ps)	$h_{p1}(t_f)$ (nm)	$x_{e2}(t_f)$ (nm)	$x'_{e2}(t_f)$ (nm)	u_{e2} (km/s)	t_{f2} (ps)	$h_{p2}(t_{f2})$ (nm)	$x'_{e2}(t_{f2})$ (nm)	$x_i(t_{f2})$ (nm)
20	1.5	4.2	16	205	181	0.28	9.5	17	183	155
26	2	5	14	209	183	0.58	10	15	186	153
43	3.8	7	7	222	191	1.5	17	8.6	200	149

time $t_r = 2.8$ ps) and the density and pressure are homogeneous and decrease with time.

Numerical results show that $\rho_{i2} = 2.44$ g/cm^3 for $P_2 = 20$ GPa and 2.28 g/cm^3 for $P_2 = 43$ GPa. As the slope of the adiabat in the two-phase region decreases as P_2 increases (see Fig. 9), the value of the corresponding adiabatic index γ and the ratio ρ_{i2}/ρ_s decrease.

A gap of density $\rho \approx 1.55$ g/cm^3 is formed between the plateau *plt 1* of the density ρ_e and a second plateau of the same density. The velocities in these two plateaus are constant, but the velocity is smaller in the second plateau. The first plateau thickness is $h_{p1} = 14$ nm and the second plateau thickness is $h_{p2} = 3$ nm. These values are in agreement with analytical results presented in Sec. II A. For our set of parameters, the time of gap formation $t_f = 5$ ps, $h_{p1} = (c_{e1} - c_{e2})t_f = 15$ nm, and $h_{p2} = (c_{e1} - c_{e2})(t - t_f) = 3$ nm for $t = 6$ ps.

The plateau size h_{p1}, the velocity u_e, and the positions x_{e2} and x'_{e2} at time t_f for three chosen values of P_2 are presented in the Table II. As the velocity $u_e \sim c_0 - c_{e1}$ and the time $t_f \sim \rho_s/\rho_e$ (see Sec. II A), u_e and t_f increase with the pressure P_2. The thickness h_{p1} of the plateau decreases as the pressure P_2 increases because the jump of the sound velocity on the isentrope decreases (see Table I).

The simulations show that for $t > t_f$, the plateau *plt 1* moves to vacuum with the constant velocity u_e. The density in the gap continues to decrease and the size of the plateau *plt 2* increases. When the front of the rarefaction wave *det 4* reaches the compressed matter, a part of the rarefaction wave *det 4* is transmitted in the compressed matter, and a part of it is reflected. The reflected wave interacts with the incident wave and a new interaction region appears in the density profile. The density in this interaction zone is equal to the density in the plateau *plt 2* at time $t_{f2} = 10$ ps. For $t > t_{f2}$, a second gap appears between the compressed matter and the plateau *plt 2* in the density profile.

The density and the velocity profiles at $t = 15$ ps are presented in Fig. 10(c). A rarefaction wave evolves in the compressed matter, and a second gap is appeared between the compressed matter and the plateau *plt 2*. The density and the velocity in two plateaus remain constant. The size of plateau *plt 1* is $h_{p1} = 14$ nm, and the size of plateau *plt 2* is $h_{p2} = 15$ nm. The density in the gap between two plateaus is $\rho \approx 0.7$ g/cm^3, and its size is larger.

The size h_{p2} of second plateau, the velocity u_{e2}, and the positions x'_{e2} and x_i, obtained in numerical simulations at time t_{f2} are also presented in Table II. The maximum size $h_{p2}(t_{f2})$ of the second plateau decreases as the initial pressure P_2 increases, while the velocity u_{e2} and the time t_{f2} increase. These results are in agreement with the analytical model presented in the previous section where $u_{e2} \sim c_{i2} - c_{e1}$, $t_{f2} \sim \rho_{i2}/\rho_e$, and $h_{p2} = (c_{e1} - c_{e2})(t_{f2} - t_f)$.

As the time goes on, the plateaus disappear, and all matter in the gaps is ejected in vacuum.

IV. DROPLETS

As we have seen in Sec. II A, a rarefaction wave propagates into the plateau with a low velocity c_{e2}. The propagation of the rarefaction front across the plateau defines an upper limit of the plateau lifetime.

When the plateaus disappear, two situations may occur. If more than half of the matter volume is occupied by liquid, the matter in the gaps is composed of vapor bubbles surrounded by liquid matter. As the time goes on, the vapor bubbles continue to grow and drive the liquid to a fragmentation. If less than half of the volume is in liquid phase, the matter in the gaps is composed of liquid droplets, which evolve in vapor. They are eventually ejected in vacuum.

In general case, the heated matter expands into an ambient gas and induces its compression. As long as the pressure in the compressed gas is lower than the pressure in the heated matter, the ambient gas has no effect on the expansion process. However, if the pressure in the compressed gas is greater than the pressure in the plateau, it slows down the matter in the plateau and drives it to a fragmentation.

The model presented above is one dimensional. It is sufficient for estimates of the liquid-vapor volume repartition in expanded matter, but it cannot predict the size of liquid droplets. A maximum size for stable droplets can be determined by the hydrodynamic disruptive and restoring forces acting on each droplet. The long term evolution of plateaus and gaps needs to be considered separately.

Concerning the plateau, two scenarios are possible depending on the pressure in the gas in the front of the plateau: either the plateau is evaporated, if the pressure in the gas is smaller than the pressure in the plateau, or it is fragmented in a liquid phase, if the pressure in the gas is greater than the pressure in the plateau. The first scenario occurs for a thin and a low-density plateau (that is, for a sufficiently high initial pressure, where the intersection point is close to the critical point). The second one occurs for a thick and a high-density plateau (that is, for a low initial pressure). Concerning the gaps, the liquid-vapor repartition depends on how fast the temperature drops down and when the droplet vaporization stops.

A. Disappearance of the plateau

The propagation of the plateau into an ambient gas induces compression of the gas in the front of the plateau.

TABLE III. Plateau disparition times and repartition of the liquid mass in the expanding cloud for three values of P_2.

P_2 (GPa)	t_{d2} (ns)	*gap 2* (%)	*plt 2* (%)	t_{d1} (ns)	*gap 1* (%)	*plt 1* (%)
20	46.3	17	25	1.3	14	29.6
26	3.7	27	15	0.7	18	23.3
43	0.054	34	6	0.033	19	5

Similarly to the shock wave analysis in Sec. II B, the density ρ_g and the pressure P_g in the compressed gas can be estimated from Eq. (5) where the velocity corresponds to the plateau velocity.

If the pressure P_g is smaller than the pressure in the plateau, the compressed gas can be neglected. The maximum sizes of the plateaus *plt 1* and *plt 2* are achieved at times t_f and t_{f2}, respectively. According to Sec. II A, the rarefaction front reaches the other side of the plateau at the time $t_{g1}=(c_{e1}/c_{e2})t_f$ for the plateau *plt 1* and at the time $t_{g2}=t_f+(t_{f2}-t_f)c_{e1}/c_{e2}$ for the plateau *plt 2*. As the sound velocity c_{e2} increases with the pressure P_2 (see Table I), and as the plateau size decreases as P_2 increases (see Table II), the lifetimes of the plateaus dramatically decrease as P_2 increases. For $P_2=20$ GPa, $t_{g1}=36.7$ ns and $t_{g2}=46.3$ ns, and for $P_2=43$ GPa, $t_{g1}=33$ ps and $t_{g2}=54$ ps.

If P_g is greater than the pressure in the plateau, the pressure of ambient gas reduces the plateau velocity. If the gas density ρ_g is smaller than the density ρ_e in the plateau, the Rayleigh-Taylor instability might appear at the interface between the plateau and the compressed gas. The instability can induce the plateau fragmentation and its premature destruction. This scenario could be operational for small initial pressures, when the plateau lifetime is relatively long.

The Rayleigh-Taylor instability of a plasma plume expanding in ambient gas was considered in Ref. 20. Although the authors were considered nanosecond laser pulses, the domain of fluences of a few tens of J/cm^2 is the same as we are interested in this study. The authors showed the instability development in the time scale of 10 ns and mixing of the plasma and gas in the thickness more than 10 μm.

Let us consider the matter in plateau and in the ambient gas in front of it as two incompressible liquids, and an interface perturbation of the initial amplitude h_0. For the Rayleigh-Taylor instability, the growth rate is expressed as $\omega_{RT}^2=-ak+\sigma k^3/\rho_e$ (Ref. 21), where σ is the surface tension and a is the acceleration. The growth rate of the instability is maximum for $k_m=\sqrt{a\rho_e/3\sigma}$. Assuming that $P_e \ll P_g$, the acceleration can be expressed as $a \sim P_g/\rho_e h_p$, where h_p is the thickness of the plateau, and then $k_m=\sqrt{P_g/3h_p\sigma}$. The amplitude of the perturbation becomes on the order of the plateau size at the time $t_{RT}=(1/|\omega_{RT}|)\ln(h_p/h_0)$. One may expect that at this time, the plateau will be divided in fragments of the size $2\pi/k_m$. These fragments evolve in the ambient gas to form liquid droplets. The size of the liquid droplets issued from the plateau fragmentation can be estimated by assuming the conservation of the mass and the volume of the fragments. Therefore, each fragment forms a liquid droplet of a radius

$$R \approx \left(\frac{3\pi h_p}{k_m^2}\right)^{1/3}. \tag{8}$$

Let us consider, as an example, an ambient gas of initial density $\rho_{ext}=10^{-3}$ g/cm^3, initial pressure $P_{ext}=10^{-4}$ GPa, and with an adiabatic index $\gamma=5/3$. For the initial pressure $P_2=20$ GPa in the heated layer, the expansion of the matter, according to Eq. (5), compresses the ambient gas to a pressure $P_g=3\times10^{-3}$ GPa and a density $\rho_g=4\times10^{-3}$ g/cm^3. For these conditions the pressure in the first plateau is $P_e=2\times10^{-4}$ GPa and the density $\rho_e=2$ g/cm^3. The pressure and the density gradients have opposite signs and the Rayleigh-Taylor instability can appear at the interface between the plateau *plt 1* and the compressed gas. The surface tension σ is supposed to be a function of the liquid temperature. The dependence $\sigma(T)=\sigma_0(1-T/T_c)^n$ is taken from Ref. 22, where T_c is the critical temperature, and σ_0 and n are two material constants. For $h_{p1}=16$ nm and $\sigma=0.52$ J/m^2, we find the unstable mode $k_m=11$ μm^{-1} and assuming $h_{p1}/h_0 \sim 3$, the instability time $t_{RT}=1.3$ ns. In this case, the time t_{RT} is smaller than the time of plateau evaporation t_{g1}. Consequently, the plateau is fragmented due to the instability and, according to Eq. (8), the radius of the formed liquid droplet is $R=107$ nm.

The plateau disparition times are estimated for three initial pressures P_2 considered in the simulations. They are presented in Table III. For $P_2=20$ and 26 GPa, the first plateau is fragmented due to the instability growth. Other plateaus disappear by expansion in vacuum.

B. Droplet size

The liquid droplets are formed from a liquid matter in the plateaus and from a liquid matter in the gaps. From the numerical results presented in Table II, one can estimate the repartition of the liquid mass in the expanding cloud at the moment of plateau disparition. This repartition is presented in Table III. For $P_2=20$ and 26 GPa, the liquid mass corresponds to 80% of the initial heated mass. The major part of the liquid matter is in the two plateaus for $P_2=20$ GPa and it is in the plateau *plt 1* and the gap *gap 2* for $P_2=26$ GPa. For $P_2=43$ GPa, only 67% of the heated mass is in the liquid state at the moment when the plateaus disappear. The major part of the liquid matter is in the gaps.

The size of a stable droplet issued from the gap or from the plateau expansion can be obtained from a balance between the dynamic pressure and the surface tension acting on each droplet.[11,23] Supposing that the velocity gradient in the gap du/dx is constant and the droplet has a spherical form,

TABLE IV. Radius of the liquid droplets, issued from the different parts of the expanding cloud.

P_2 (GPa)	*gap 2* (GPa)	*plt 2* (nm)	*gap 1* (nm)	*plt 1* (nm)
20	2136	426	187	107
26	380	258	122	75
43	19	22	11	11

its kinetic energy can be estimated as $W_k=(1/2)\rho V[u_0^2+(1/5)R^2(du/dx)^2]$, where $V=4\pi R^3/3$ is the droplet volume and R is the droplet radius. Estimating then the energy of surface tension as $W_s=4\pi R^2\sigma=3\sigma V/R$, one can find the maximum droplet radius from the condition of the minimum of the droplet energy density, $(W_k+W_s)/V$, as follows:

$$R=\left[\frac{15\sigma}{\rho(du/dx)^2}\right]^{1/3}. \tag{9}$$

The radius of droplets formed in different parts of the expanding cloud for the initial pressures in the heated layer is presented in Table IV. The average size of the droplets formed by the plateau fragmentation (*plt 1* for $P_2=20$ and 26 GPa) is estimated with Eq. (8). The size of droplets issued from the plateau expansion (*plt 2* for all values of P_2 and *plt 1* for $P_2=43$ GPa) is estimated by using Eq. (9) with the velocity gradient in the rarefaction wave and the liquid density in the plateau. The dependence $\sigma(T)$ has been taken from Ref. 22 according to the discussion presented in Sec. IV A.

For each pressure, the bigger droplets are formed in the second gap (*gap 2*). As the velocity gradient is smaller in this gap, the droplet size is greater. This result is confirmed by recent simulations[16,17] and experiments.[13] The simulations indicate that the bigger droplets are formed near the target surface. In the experiments, two populations of droplets are observed: small droplets that are more abundant in the fast expanding cloud and larger particles that are located mostly at the back. Table IV shows that the average droplet radius decreases as the pressure P_2 increases. The sound velocity c_{e2} increases with P_2, while the plateau size decreases. Therefore, the plateau lifetime decreases as P_2 increases, the velocity gradients in the different parts of the expanding cloud are greater, and the droplet sizes decreases.

Our theoretical estimates of the droplet formation can be compared with experiments. The homogeneously heated thin films are the most appropriate object for such a comparison as the thermal conductivity was neglected in our simulations. In the experiment reported in Ref. 12, the authors found that the average nanoparticle radius decreases as the laser fluence increases as long as the matter evolution can be described by a single temperature. For greater fluences, a double-temperature adiabatic expansion takes place. In this case, the liquid-vapor phase transition occurs for a smaller ion temperature and according to our model, the average droplet radius increases.

V. CONCLUSION

We presented a complete study of the relaxation process of an isochoric liquid layer at a target surface that accounts for a liquid-vapor phase transition. The consecutive steps of the relaxation process are described by an analytical model. The density profile of expanding layer is nonmonotonic due to the transformation of a part of heated matter in a liquid-vapor mixture. Liquid layers in the expanding flow have a thickness of a few tens of nm and a velocity up to a few km/s.

The theoretical analysis is confirmed by numerical simulations performed for three different initial pressures in a hot layer on a surface of an aluminum target. The matter is described by the multiphase equation of state by Bushman *et al.*[19] The evolution of the expanding cloud agrees with the predictions of the analytical model. The repartition of the liquid and vapor in the expanding matter is estimated, and the maximum liquid droplet sizes are determined. The estimate of the liquid droplet sizes is in agreement with recent numerical and experimental results.[12,13,16,17] The larger droplets are formed near the target surface, while the smaller droplets are formed in the front of the expanding flow. Moreover, the average droplet size decreases as the initial pressure increases.

Our simple analysis provides a general framework of the matter evolution during the relaxation with phase transition. In a more realistic description, one should account for the target expansion during the heating process and for the heat conduction. Moreover, several shock waves may be launched into the matter with a continuous delay time. In this case, several plateaus of different densities may be formed in the expanding cloud as it was observed in the numerical simulations performed in Ref. 4. The densities of these plateaus correspond to the crossing points of the relaxation curves with the binodal. Although the analysis of the expansion process is more complicated, our general approach remains valid as well as the estimates for the liquid-vapor mass repartition and for the droplet size.

*chimier@lp3.univ-mrs.fr

[1] N. A. Inogamov, S. I. Anisimov, and B. Retfeld, JETP **88**, 1143 (1999).

[2] N. A. Inogamov, Yu. V. Petrov, S. I. Anisimov, A. M. Oparin, N. V. Shaposhnikov, D. von der Linde, and J. Meyer-ter-Vehn, JETP Lett. **69**, 310 (1999).

[3] S. I. Anisimov, N. A. Inogamov, A. M. Oparin, B. Rethfeld, T. Yabe, M. Ogawa, and V. E. Fortov, Appl. Phys. A **69**, 617 (1999).

[4] F. Vidal, T. W. Johnston, S. Laville, O. Barthélemy, M. Chaker, B. LeDrogoff, J. Margot, and M. Sabsabi, Phys. Rev. Lett. **86**, 2573 (2001).

[5] E. G. Gamaly, A. V. Rode, B. Luther-Davies, and V. T. Tikhonchuk, Phys. Plasmas **9**, 949 (2002).

[6] J. P. Colombier, P. Combis, F. Bonneau, R. Le Harzic, and E. Audouard, Phys. Rev. B **71**, 165406 (2005).
[7] B. Chimier, V. T. Tikhonchuk, and L. Hallo, Phys. Rev. B **75**, 195124 (2007).
[8] M. E. Povarnitsyn, T. E. Itina, M. Sentis, K. V. Khishchenko, and P. R. Levashov, Phys. Rev. B **75**, 235414 (2007).
[9] P. Lorazo, L. J. Lewis, and M. Meunier, Phys. Rev. B **73**, 134108 (2006).
[10] D. S. Ivanov and L. V. Zhigilei, Phys. Rev. Lett. **98**, 195701 (2007).
[11] S. Amoruso, G. Ausanio, R. Bruzzese, M. Vitiello, and X. Wang, Phys. Rev. B **71**, 033406 (2005).
[12] S. Eliezer *et al.*, Phys. Rev. B **69**, 144119 (2004).
[13] S. Noël, J. Hermann, and T. Itina, Appl. Surf. Sci. **253**, 6310 (2007).
[14] L. D. Landau and E. M. Lifshitz, *Fluid Mechanics* (Pergamon, Oxford, 1987), Vol. 6.
[15] Y. B. Zel'dovich and Y. P. Raizer, *Physics of Shock Waves and High-Temperature Hydrodynamic Phenomena* (Academic Press, London, 1967), Vol. 1.
[16] T. E. Itina, K. Gouriet, L. V. Zhigilei, S. Noël, J. Hermann, and M. Sentis, Appl. Surf. Sci. **253**, 7656 (2007).
[17] L. Zhigilei, Appl. Phys. A **76**, 339 (2003).
[18] E. Lescoute, L. Hallo, B. Chimier, V. T. Tikhonchuk, D. Hébert, J.-M. Chevalier, B. Etchessahar, and P. Combis, Phys. Plasmas **15**, 063507 (2008).
[19] A. V. Bushman, I. V. Lomonosov, and V. E. Fortov, Sov. Technol. Rev. B **5**, 1 (1993).
[20] K. Rifai, F. Vidal, and T. W. Johnston, Phys. Plasmas **14**, 082311 (2007).
[21] A. R. Choudhuri, *The Physics of Fluids and Plasmas* (Cambridge University Press, Cambridge, England, 1998).
[22] B. C. Allen, *Liquid Metals, Chemistry and Physics* (Marcel Dekker, New York, 1972), Chap. 4, pp. 161–212.
[23] D. E. Grady, J. Appl. Phys. **53**, 322 (1982).